*8484–8498* *Nucleic Acids Research, 2012, Vol. 40, No. 17* *Published online 22 June 2012*
*doi:10.1093/nar/gks598*

# NMDAR signaling facilitates the IPO5-mediated nuclear import of CPEB3

**Hsu-Wen Chao[1], Yen-Ting Lai[1,2], Yi-Ling Lu[1], Chi-long Lin[3], Wei Mai[3] and Yi-Shuian Huang[1,2,*]**

[1]Institute of Biomedical Sciences, Academia Sinica, Taipei 11529, Taiwan, [2]Graduate Institute of Microbiology, National Taiwan University, Taipei 10051, Taiwan and [3]National RNAi Core Facility, Academia Sinica, Taipei 11529, Taiwan

Received May 1, 2012; Revised May 23, 2012; Accepted May 28, 2012

## ABSTRACT

**Cytoplasmic polyadenylation element-binding protein (CPEB)3 is a nucleocytoplasm-shuttling RNA-binding protein and predominantly resides in the cytoplasm where it represses target RNA translation. When translocated into the nucleus, CPEB3 binds to Stat5b and downregulates Stat5b-dependent transcription. In neurons, the activation of *N*-methyl-D-aspartate receptors (NMDARs) accumulates CPEB3 in the nucleus and redistributes CPEB3 in the nucleocytoplasmic compartments to control gene expression. Nonetheless, it is unclear which karyopherin drives the nuclear import of CPEB3 and which transport direction is most affected by NMDA stimulation to increase the nuclear pool of CPEB3. Here, we have identified that the karyopherins, IPO5 and CRM1, facilitate CPEB3 translocation by binding to RRM1 and a leucine-containing motif of CPEB3, respectively. NMDAR signaling increases RanBP1 expression and reduces the level of cytoplasmic GTP-bound Ran. These changes enhance CPEB3–IPO5 interaction, which consequently accelerates the nuclear import of CPEB3. This study uncovers a novel NMDA-regulated import pathway to facilitate the nuclear translocation of CPEB3.**

## INTRODUCTION

Long-term memory involves the activity-induced synthesis of plasticity-related proteins in neurons to support long-lasting morphological and functional changes of synapses. This type of activity-driven gene expression is regulated at both transcriptional and translational levels (1–3). Previous research has shown that proteins enriched at or near neuronal synapses accumulate in the nucleus in response to stimulation. These proteins include factors controlling gene expression, scaffold molecules, and the proteolyzed intracellular domains of synaptic receptors (4,5). Transcription factors, such as cyclic AMP responsive element-binding protein (CREB)2, and translation regulators, such as cytoplasmic polyadenylation element-binding protein (CPEB)3 and CPEB4, move to the nucleus after activation of the *N*-methyl-D-aspartate receptor (NMDAR) (6–9), suggesting that the nucleocytoplasmic partition of these proteins by specific neuronal signaling determines their role in gene expression.

Synapse-to-nucleus communication (i.e. retrograde trafficking of protein molecules from synaptic areas to the nucleus) plays an important role in synaptic plasticity, long-term memory, circadian rhythms and neuronal survival (4,10). However, the molecular machineries, including signal initiators and nucleocytoplasmic translocators, responsible for redistributing these synaptic proteins are less characterized. Although the small proteolyzed intracellular domains of receptors can passively diffuse into the nucleus, proteins with a molecular weight exceeding 40 kDa generally require the assistance of karyopherins for nuclear localization (11). Importins α1, α2 and β1 of the nuclear import machinery are present at somatodendritic regions, and stimulation of neurons with NMDA increases the nuclear translocation of all three importins (12). Importins α and β, in conjunction with nucleocytoplasm translocation regulators such as Ras-related nuclear protein (Ran) and Ran-binding protein (RanBP)1, are also present in the axoplasm of sciatic nerves (13). After nerve injury, the expression of importin β and RanBP1 are upregulated (13) that may help deliver transcription factors, such as signal transducer-activated transcription (Stat)3, to the nucleus (14). The accumulation of nuclear CREB2 via importin α1/6-mediated translocation appears in neurons treated with NMDA to induce chemical long-term depression (c-LTD) (8). NMDAR signaling also induces nuclear localization of Jacob by importin α1-facilitated translocation (7,15). Thus, activity-regulated import pathways appear to play a critical role in transporting neuronal

*To whom correspondence should be addressed. Tel: +886 22652 3523; Fax: +886 22785 8594; Email: yishuian@ibms.sinica.edu.tw

signals from distal dendrites and axons into the nucleus to control gene expression.

CPEB family proteins, including CPEBs1–4, regulate the translation of target-specific RNAs and reside predominantly in the cytoplasm. Recent research has identified that CPEBs 2 and 3, repress translation elongation through an interaction with eEF2 and stimulate translation in response to arsenite (16) or NMDA (17) in a polyadenylation-independent manner. Despite the cytoplasmic role of CPEBs in regulating translation, recent studies have shown that all CPEBs accumulate in the nucleus when chromosome region maintenance (CRM)1-dependent export is blocked by leptomycin B (LMB) in various cells, indicating that CPEBs are nucleocytoplasm-shuttling proteins (6,9,18). Interestingly, CPEB3 and CPEB4 accumulate in the nucleus in NMDA-stimulated neurons (6,9). Although CPEB4's function in the nucleus is unclear, the nuclear form (i.e. export-defective mutant) of CPEB4 has a less protective effect in neurons deprived of oxygen and glucose (6), a cellular model that mimics ischemia-induced neuronal death (19,20). In contrast, CPEB3 can interact with Stat5b and inhibit Stat5b-dependent transcription in the nucleus (9). Nonetheless, it remains elusive whether the source of elevated nuclear CPEB3 is contributed by a change in import or export in NMDA-stimulated neurons and whether specific karyopherins are involved to facilitate nuclear translocation of CPEB3. Although CPEB3, with a molecular weight of 76 kDa, likely needs an active import mechanism to transit across the nuclear pore complex, *in silico* analysis does not reveal any canonical nuclear localization sequence (NLS) in CPEB3.

Using various CPEB3 mutants and small hairpin RNA (shRNA) knockdown screening, we have identified two *cis*-elements of CPEB3, the LENSL motif and RNA-recognition motif (RRM)1, control CPEB3's nucleocytoplasmic distribution through interaction with CRM1 and importin 5 (IPO5), respectively. Time-lapse live imaging and biochemical experiments suggest that NMDA-increased RanBP1 expression presumably activates Ran's GTPase. The conversion of GTP-bound (RanGTP) to GDP-bound Ran (RanGDP) facilitates IPO5's binding to CPEB3 and increases the nuclear translocation of the Ran–IPO5–CPEB3 complex to elevate nuclear CPEB3 level.

## MATERIALS AND METHODS

### Antibodies and chemicals

Antibodies used in the study are MAP2 (cat No. NB300-213) from Novus Biologicals; Ran (cat No. 53817) from AnaSpec; RanGTP (cat No. 26915) from NewEast Biosciences; lamin B (cat No. sc-6217), CRM1 (cat No. sc-74454) and IPO5 (cat No. sc-17802) from Santa Cruz Biotechnology; synaptophysin (Sy38, cat No. MAB5258) from Millipore; RanBP1 (cat No. GTX103192) from GeneTex; GFP (cat No. G1544), β-actin (cat No. A5441), α-tubulin (cat No. T5168) and flag epitope (cat No. F1804) form Sigma-Aldrich. The CPEB3 monoclonal antibody was raised using the N-terminal 427 amino acids (a.a.) of hCPEB3 produced in *Escherichia coli*. With the exception of LMB (cat No. sc-202210) from Santa Cruz Biotechnology, all other chemicals were purchased from Sigma-Aldrich. The fluorescein isothiocyanate (FITC)-conjugated donkey anti-chicken IgY (cat No. 703-095-155) was from Jackson ImmunoResearch. The AlexaFluor-conjugated secondary antibodies were obtained from Invitrogen.

### Plasmid construction

The shRNA clones, TRCN0000101931 (GCCCATGATT AAGGAACACAT) and TRCN0000101932 (GCTTCAT TTAAGTATGCAGAA), targeted against mouse IPO5 were purchased from the RNAi Core Facility (Academia Sinica). The various deleted human CPEB3 fragments were cloned into the pcDNA3.1-myc plasmid. The pQE30-IPO5 was used as the template to amplify full length and truncated human IPO5 fragments for cloning into the pcDNA3.1-flag and pEGFP-C1 plasmids. The pcDNA3.1-flag-RanT24N was generated by site-directed mutagenesis using the pcDNA3.1-flag-Ran as the template.

### Cell culture, lentivirus production and DNA transfection

All experimental protocols using mouse or rat brains for primary cultures were carried out following guidelines of the Institutional Animal Care and Utilization Committee. The papain solution (0.6 mg/ml papain and DNaseI, 0.5 mM ethylenediaminetetraacetic acid (EDTA), 0.2 mg/ml cysteine and 1.5 mM $CaCl_2$ in 1 × HBSS buffer) was used to dissociate cerebral cortices or hippocampi isolated from embryonic day 19 mouse or rat pups. Cortical and hippocampal neurons were cultured in Neurobasal medium with 1 × B27 supplement (21,22). HEK293T, HeLa and Neuro-2a cells were cultured in Dulbecco's modified Eagle medium supplemented with 10% fetal bovine serum. Lentivirus particles were generated using Virapower packaging system (Invitrogen). Transfection of plasmid DNAs to cell lines was carried out using lipofectamine 2000 (Invitrogen) following the manufacture's protocol.

### UV-crosslinking RNA-binding assay

The 6-cm dish of 293 T cells expressing myc-tagged CPEB3 variants was lysed in 150 µl of 2X gel retardation buffer (20 mM Hepes, pH 7.4, 100 mM KCl, 2 mM $MgCl_2$, 0.1% TritonX-100, 10% glycerol and 0.5 mM DTT). The 1904 RNA probe identified previously as the CPEB3-binding sequence was labelled by *in vitro* transcription with $\alpha^{32}$P-UTP (17). Twenty microlitre reactions containing $10^5$ counts per minute of labelled RNA, 50 µg heparin, 1 µg yeast tRNA and 10 µl of 293T-cell lysate were kept on ice or 15 min, and then irradiated with 1200 J of UV (254 nm) light for 10 min. The UV-crosslinked samples were treated with 200 ng of RNase A at 37°C for 10 min and resolved by sodium dodecyl sulphate–polyacrylamide gel electrophoresis (SDS–PAGE).

### ShRNA knockdown screening, high content image acquisition and analysis

Mouse cortical neurons were resuspended at the density of $2 \times 10^5$ cells/ml in the Neurobasal medium with 1 × B27 supplement. One hundred microlitres of the cell suspension was dispensed to 96-well poly-D-lysine-coated plates (BD Bioscience) using MicroFill Microplate Dispenser (BioTek). The lentiviral particles expressing 174 shRNAs against the selected targets along with nine control lentiviruses were produced and arrayed in two 96-well plates in the RNAi core facility. All multi-well pipetting steps were performed using a Biomek NXR Liquid Handling Workstation (Beckman Coulter) in the core facility. Cortical neurons of days *in vitro* (DIV) 7 were infected with 5 µl of viral medium (average titer: $1.48 \pm 0.44 \times 10^4$/µl). After overnight incubation, each well was changed with 100 µl of fresh cultured medium. On DIV 9, 10 µl of medium with or without 5.5 µg/ml of puromycin was added to each well. Three days after puromycin selection (DIV 12), the infected neurons were stimulated with or without 20 µM NMDA for 30 min prior to fixation and immunostaining. Unless otherwise specified, all procedures were carried out at room temperature and with 100 µl of solution dispensed and aspirated to each well using the automatic system. Total 10 plates of neurons were fixed with 4% formaldehyde for 20 min, washed three times with phosphate buffered saline (PBS), permeabolized with 0.2% TritonX-100 in PBS for 5 min, washed twice with PBS and incubated with the blocking buffer (10% horse serum in PBS) for 30 min. The solution was then changed with 50 µl of primary antibody solution (MAP2 and affinity-purified polyclonal CPEB3 antibodies in the blocking buffer) and incubated overnight at 4°C. The neurons were washed three times with PBS and incubated with 50 µl of secondary antibody solution (FITC-conjugated anti chicken IgY, AlexaFluor 594-conjugated anti rabbit IgG and 4′-6-diamidino-2-phenylindole (DAPI) in the blocking buffer) for 1 h. After three PBS washes, the immunostained neurons were stored in 0.02% sodium azide in PBS and analysed by Cellomic AarrayScan VTI HCS reader. Twenty center fields of images were acquired with a 20× objectives and three colour channels for DAPI, FITC and AlexaFluor 594. The 'Cytoplasm to Nucleus' BioApplication software was used to analyse images.

### Co-immunoprecipitation

To examine CPEB3–IPO5–Ran association in neurons, $8 \times 10^6$ cortical neurons of DIV 16 were treated with 3 min of 50 µM NMDA and then incubated for the designated time prior to 4% formaldehyde crosslinking at room temperature for 5 min. The fixed neurons were lysed in 1.5 ml buffer (10 mM Hepes, pH 7.5, 320 mM sucrose, 5 mM EDTA, 5 mM DTT, 10 µM MG132, 1% TritonX-100, 0.5% sodium deoxychlorate, 0.1% SDS, 1 × protease and phosphatase inhibitors (Roche)) at 4°C for 60 min, followed by sonication for 10 s and then centrifugation at 13 000 rpm for 30 min. The supernatant was divided, diluted with one volume of $H_2O$, incubated with 30 µl protein G beads bound with 5 µg of CPEB3 or IPO5 IgG at 4°C for 6 h. The beads were then washed with cold PBST (1% TritonX-100 in PBS) for three times and the precipitated proteins were eluted with Laemmli sample buffer at 95°C for 10 min and used for western blot analysis. To study the binding motifs required for CPEB3–IPO5 interaction and the complex formation of CPEB3, IPO5 and Ran, the transfected HeLa cells of 60-mm dish were lysed in 1 ml above buffer without SDS and deoxycholate. The following procedures without sonication were similar except using beads bound with GFP, myc or flag IgG.

### Immunostaining, confocal image acquisition and quantification

The transfected cells or infected neurons treated with LMB or NMDA for the indicated conditions were washed two times with PBS and fixed with 4% formaldehyde and 4% sucrose in PBS for 10 min at room temperature. After permeabolization with cold methanol at −20°C for 15 min, cells were blocked with 10% bovine serum albumin in PBS for 2 h at room temperature and probed with designated antibodies at 4°C for overnight. After several washes, the proper Alexa Fluor-conjugated secondary antibodies and DAPI were added and incubated for 1 h at room temperature. HeLa cells and neurons rinsed with three times of PBS were mounted with Vectashield medium (Vector Laboratories). Acquisition of fluorescent images was performed using LSM510META confocal microscope (Carl Zeiss) with a Plan-Apochromat 63X/1.25 NA oil objective lens. For analyzing the nucleocytoplasmic signals of DAPI, CPEB3, MAP2 and IPO5 in fixed neurons, each image was consisted of a stack of 7–9 Z-series images of 0.5 µm spacing. The images were analysed and quantified using Zeiss LSM510, version 4.2 SP1 software. For live-cell recording, the coverslip of DIV 15–18 neurons expressing EGFP-CPEB3 was transferred from a culture dish to POC-R cell cultivation system (LaCon) and equilibrated in the live-cell recording chamber of 5% $CO_2$ at 37°C for at least 2 h. Time-lapse live images were acquired every 3 min for 30 min prior to LMB or NMDA stimulation and then continuously recorded for another 80–90 min. The images were processed and analysed using ImageJ software (National Institute of Health). The data were exported to Excel and GraphPad Prism for analyses and expressed as mean ± standard error of the mean (SEM). The statistical significance was determined by Student's *t*-test.

### Nuclear and cytoplasmic fractionation

Nucleocytosolic fractions of cultured neurons were prepared using ProteoJET Cytoplasmic and Nuclear Protein Extraction Kit (Fermentas). Cortical neurons of DIV 18 in 100-mm dishes were treated with 50 µM NMDA for 3 min and then incubated for 30 min before lysis with 1 ml cell lysis buffer with the addition of 5 mM DTT, 1 × protease and phosphatase inhibitor cocktails (Roche). The cell lysates were incubated on ice for 10 min and then homogenized with Dounce homogenizer using loose pestle (Wheaten) for 50 strokes. The lysates

were vortexed for 10 s and incubated on ice for 10 min prior to centrifugation at 500 × *g* for 5 min at 4°C. The supernatants were collected and spun again at 5000 rpm for 5 min. The supernatants were harvested and centrifuged at 10 000 rpm for 30 min to obtain the clear cytoplasmic extract. The pellets collected from the first two centrifugations were rinsed with 0.5 ml of nuclei washing buffer with the addition of 5 mM DTT, 1 × protease and phosphatase inhibitor cocktails, vortexed for 10 s, incubated on ice for 5 min before centrifugation at 500 × *g* for 5 min. The resulting pellets were washed two more times to obtain the high purity nuclei for extract preparation.

### Calcium phosphate DNA transfection

Delivery of DNA into neurons was performed by calcium phosphate transfection (23). For DIV 10–12 neurons grown on 18-mm coverslip in a 12-well plate, 0.5 ml medium/well was kept. The 3 μg plasmid DNA was mixed with 5 μl of 2.5 mM $CaCl_2$ and $H_2O$ to the volume of 50 μl before adding 50 μl of 2 × HeBS dropwise with brief vortex. The DNA mixture was incubated at room temperature for 20 min and then added dropwise to cultured neurons. For neurons cultured on 60-mm dish, 2 ml medium was left and the DNA mixture (10 μg DNA, 125 μM $CaCl_2$ in 500 μl 1 × HeBS) prepared in the same way was applied to cultures. The neurons were incubated in 5% $CO_2$ at 37°C for 2 h before washing with medium three times in 10% $CO_2$ at 37°C for 10 min to remove residual calcium phosphate precipitates. The washed neurons were then cultured in a 5% $CO_2$ incubator until ready for experiments.

## RESULTS

### Identification of nuclear import and export sequences of CPEB3

The pharmacological blockade of CRM1-dependent export by LMB induces the nuclear accumulation of CPEB3 in neurons and ectopically expressed CPEB3 in many cell lines (9), so we used HeLa cells to identify the non-canonical nuclear export sequence (NES) and NLS of CPEB3. Figure 1A shows the various myc-tagged CPEB3 mutants used in the study. The expression and RNA-binding ability of these mutants were examined by western blotting (Figure 1B) and UV-crosslinking RNA-binding assay (Figure 1C), respectively. Myc-CPEB3 migrates to the position of 100 kDa higher than its calculated molecular weight of 76 kDa. The N-terminal a.a. of CPEB3 seem to account for its unusual mobility, because mutN (427 a.a.) migrates more slowly than mut4 (469 a.a.) and mut8 (533 a.a.) migrates more slowly than mut3 (551 a.a.) on SDS–PAGE. The mutants with a deletion in the RNA-binding domain (RBD), including mut7, mut8 and mutN, cannot bind to the 1904 RNA probe (Figure 1C). The HeLa cells expressing various CPEB3 mutants were treated with or without LMB for 30 min prior to immunostaining with myc antibody. In this test, the NES-deficient mutants are expected to show elevated nuclear distribution, whereas the NLS-lacking mutants should exhibit reduced nuclear signals after LMB treatment. MutC and mut6 accumulated in the nucleus without LMB, indicating that a.a. 318–425 is essential to maintain CPEB3 in the cytoplasm. Recent research shows that the two leucines in the LESSL motif of CPEB4 are required for its nuclear export (6). Because a similar $L_{349}ENSL_{353}$ motif appears in the a.a. 318–425 of CPEB3, we made the $A_{349}A_{353}$ mutant and found that the LENSL motif was essential for nuclear export of CPEB3 (Figure 1D). The nuclear distribution of mutC could be caused simply by diffusion because of its small size. Alternatively, the RBD region may contain an NLS. Thus, two additional RNA binding-deficient mutants, mut7 and mut8, were analysed. Only mut7 exhibited import deficiency in the presence of LMB, indicating that the NLS is located in the RNA recognition motif (RRM)1. Approximately 80–100 transfected cells were analysed using MetaMorph image software to quantify the nuclear distribution of wild-type (wt), mut6, mut7 and mut8 CPEB3. The nuclear signal of mut7 is slightly (~10%) but significantly elevated after LMB treatment (Figure 1E). In addition, the RRM1-deleted mutN was nuclearly accumulated in the presence of LMB, suggesting that potentially a cryptic NLS is located in the N-terminus of CPEB3.

### NMDA-induced nuclear accumulation of CPEB3 depends on RRM1

To test whether the NMDA-accumulated nuclear pool of CPEB3 also relies on the NLS in the RRM1, neurons infected with lentiviruses expressing wt, export (mut6), or import (mut7) mutant CPEB3 were stimulated with NMDA and then immunostained with myc antibody (Figure 2A). Most unstimulated neurons showed a relatively strong CPEB3 signal in the cytoplasm, with less than 10% of cells displaying nuclear distribution. NMDA induced 50% of cells to exhibit strong CPEB3 signals in the nucleus (Figure 2B). In contrast, the export (mut6) and import (mut7) mutants in approximately 90% of neurons showed nucleus- and cytoplasm-distributed patterns, respectively, regardless of NMDA treatment (Figure 2B). Thus, the LENSL motif and RRM1 of CPEB3 also function as NES and NLS in neurons.

### Functional shRNA knockdown screening to search for the *trans*-acting factors in controlling nucleocytoplasmic shuttling of CPEB3

To identify the karyopherin that facilitates the import of CPEB3, we first focused on importins α1 and β1, the nuclear translocation of which increases in response to NMDA stimulation (12). However, co-immunoprecipitation (co-IP) assay failed to detect any interaction between CPEB3 and either importin. This may be because CPEB3 does not contain a classical NLS to be recognized. Because all karyopherins, including importins and exportins, display expression patterns in most tissues according to the UniGene EST expression profiles, we selected available shRNAs from the RNAi Consortium (TRC) mouse database (24) that were targeted against

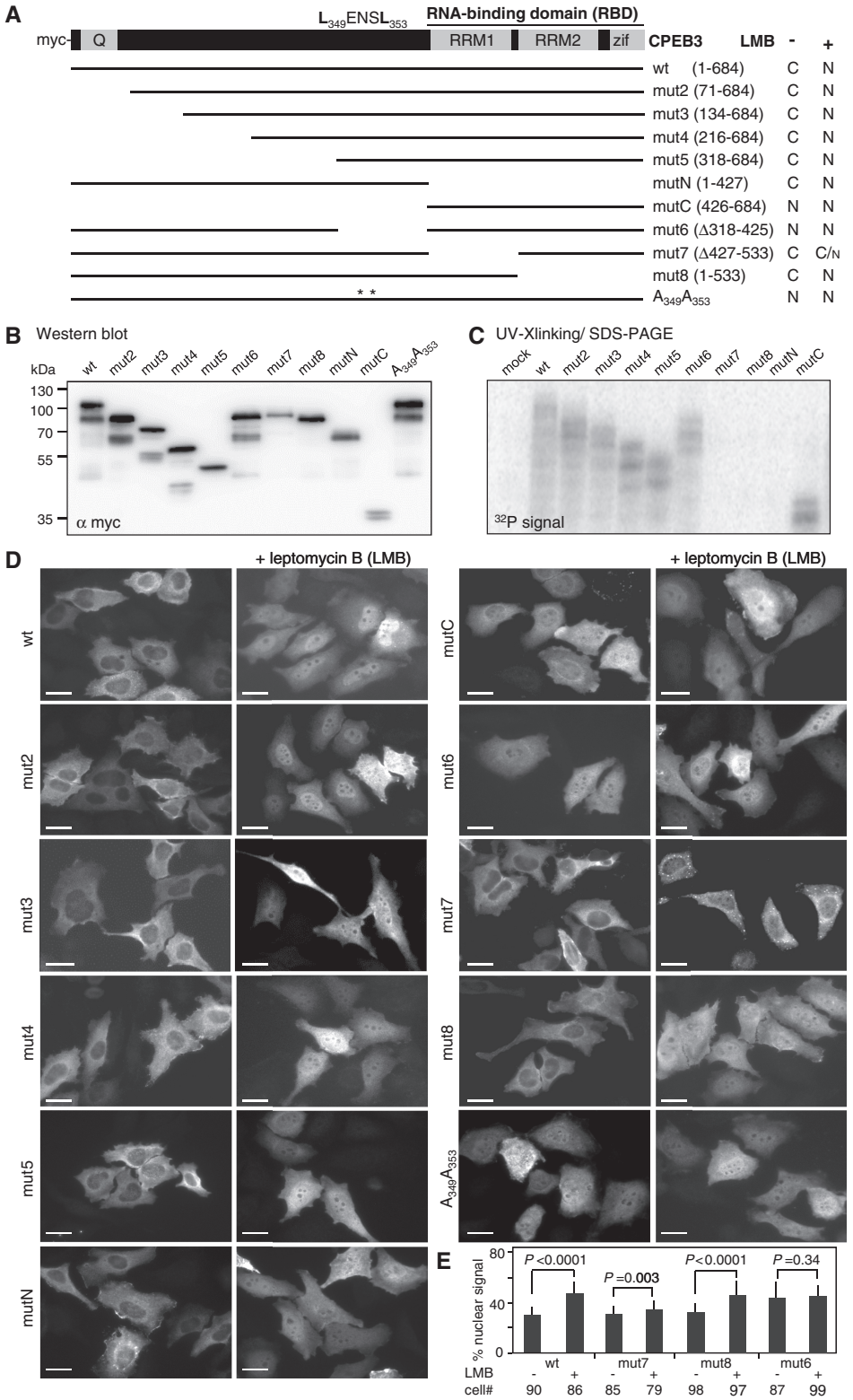


**Figure 1.** Identification of the *cis*-elements required for nucleocytoplasmic translocation of CPEB3. (**A**) Salient features of CPEB3, showing the N-terminal glutamine-rich region (Q) and the C-terminal RNA-binding domain (RBD) composed of two RNA recognition motifs (RRM) and zinc fingers (Zif). The LENSL motif is the nuclear export sequence. The various myc-tagged CPEB3 mutants are illustrated. The 293 T lysates containing wild-type (wt) and mutant (mut) CPEB3 were (**B**) used for western blotting or (**C**) crosslinked with radiolabelled RNA probe for RNA-binding assay. (**D**) HeLa cells expressing wt and mut CPEB3 were treated with ± 10 ng/ml LMB for 30 min prior to fixation and immunostaining with myc antibody. Subcellular localizations of wt and mut CPEB3 proteins in ± LMB-treated cells are summarized in (A), N: nucleus; C: cytoplasm. Scale: 20 μm (**E**) To quantify nuclear distribution of mut6, mut7, mut 8 and wt CPEB3, ~80–100 transfected cells ± LMB treatment were analysed using MetaMorph software. The nuclear CPEB3 signal was divided by total cellular signal to yield the % nuclear signal. Error bars indicate SD. Statistical analysis was performed using Student's *t*-test.

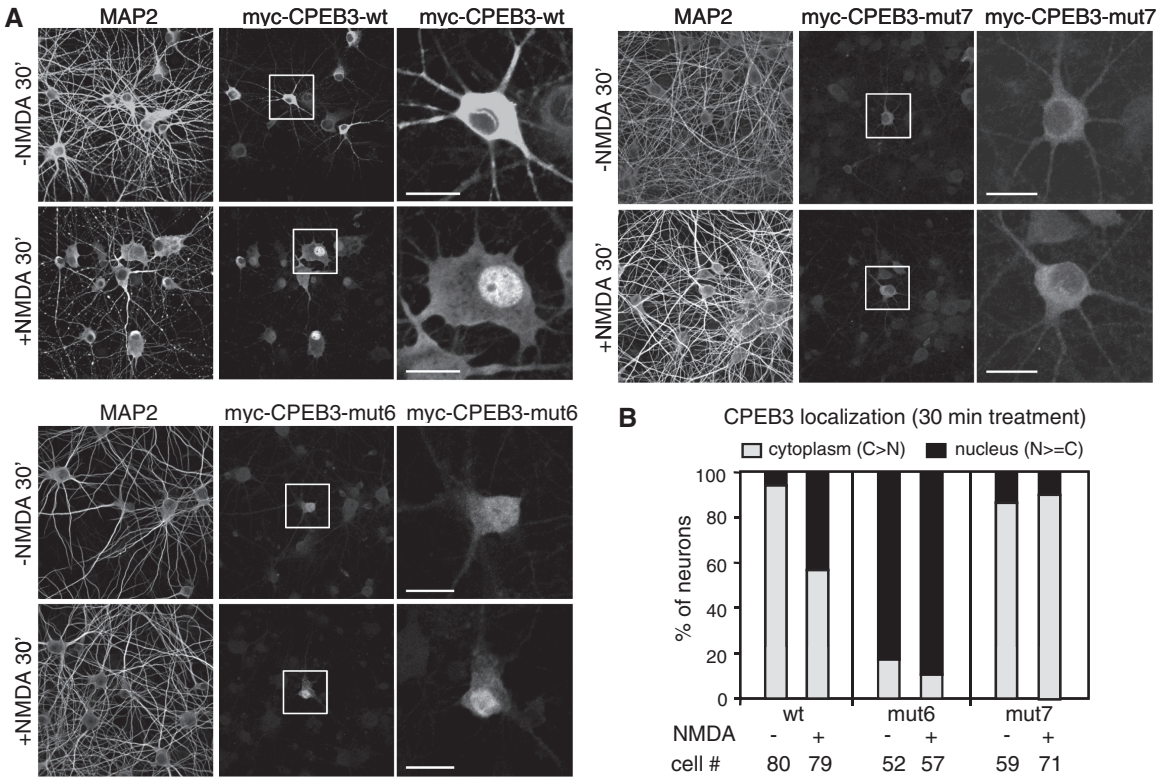


**Figure 2.** Deletion of NLS in CPEB3 affects its nuclear accumulation in NMDA-treated neurons. (**A**) Neurons infected with lentivirus expressing myc-tagged wt, mut6 or mut7 CPEB3 were stimulated with or without 50 μM NMDA for 30 min before immunostaining with myc and MAP2 antibodies. Scale: 20 μm. (**B**) The localization of CPEB3 wt, mut6 and mut7 in neurons was analysed. A staining signal in the cytoplasm exceeding that in the nucleus is considered as cytoplasm-localized (light grey bar), and the rest is grouped as nucleus-localized (dark grey bar).

karyopherins and some nuclear translocation regulators. For example, Ran is a small GTPase involved in the transport of proteins across the nuclear envelope by modulating karyopherin's ability to bind or release cargo molecules (25). A Ran GTPase-activating protein (GAP), RanGAP1, and a Ran guanine nucleotide exchange factor (GEF), RCC1 (i.e. regulator of chromosome condensation 1), are primarily localized in the cytoplasm and the nucleus, respectively, to cycle Ran's nucleotide-bound state between RanGDP and RanGTP (25–27). These regulatory proteins were also included in the screening. The lentiviruses expressing the 174 selected shRNAs against 35 targets and the control viruses were produced and arrayed in two 96-well plates. Supplementary Table S1 lists the information of 174 shRNAs. Each plate of viruses was used to infect five 96-well plates of mouse cortical neurons of DIV 7. On DIV 9, puromycin was added to four plates to kill non-infected neurons and one plate was left untreated (Figure 3A). On DIV 12, two puromycin-selected plates were stimulated with or without NMDA for 30 min and then fixed for CPEB3, microtubule-associated protein (MAP)2 and DAPI staining (representative images shown in Figure 3B). The DAPI and MAP2 signals define the nucleus and the somatodendritic cytoplasm, respectively. The CPEB3 signal in the DAPI-outlined region divided by that in the MAP2-stained somatocytoplasmic area is the $N/C$ ratio (Figure 3A). The cell numbers and $N/C$ ratios of 174 shRNA-targeted wells were averaged and displayed as mean ± SD (Figure 3C and D). The mean cell number in puromycin-treated plates is 60–70% less than that in the non-treated plate (Figure 3C). A positive correlation between the cell number and viral titer in each well of puromycin-selected plates is found (Supplementary Figure S1), indicating that lower cell density is mainly caused by less viral infection. Nonetheless, the two sets of infected neurons (puro +) and one set of unselected neurons (puro-) have similar mean $N/C$ ratios. In contrast, NMDA treatment significantly increases the mean $N/C$ ratio (Figure 3D). To determine whether the variability in cell density affects the $N/C$ ratio of CPEB3 that may compromise the data interpretation, the average cell number was plotted against the mean $N/C$ ratio in each shRNA-targeted well from duplicate datasets with or without NMDA stimulation. The lack of a diagonal distribution pattern indicates that the $N/C$ ratio of CPEB3 is generally not influenced by neuronal density (Figure 3E). The N/C ratios of 174 shRNA-targeted and NMDA-treated neurons are arranged in increasing order (red line) and the ratio of its untreated counterpart (Ctrl) is plotted accordingly in blue (Figure 3F). Figure 3G lists the $N/C$ ratios in NMDA-treated neurons falling beyond 95% confidence interval for the mean (i.e. mean ± 1.96 SD). Tnpo1 and Phax are shown in light grey because of the large variation from the duplicate datasets. In the list, the

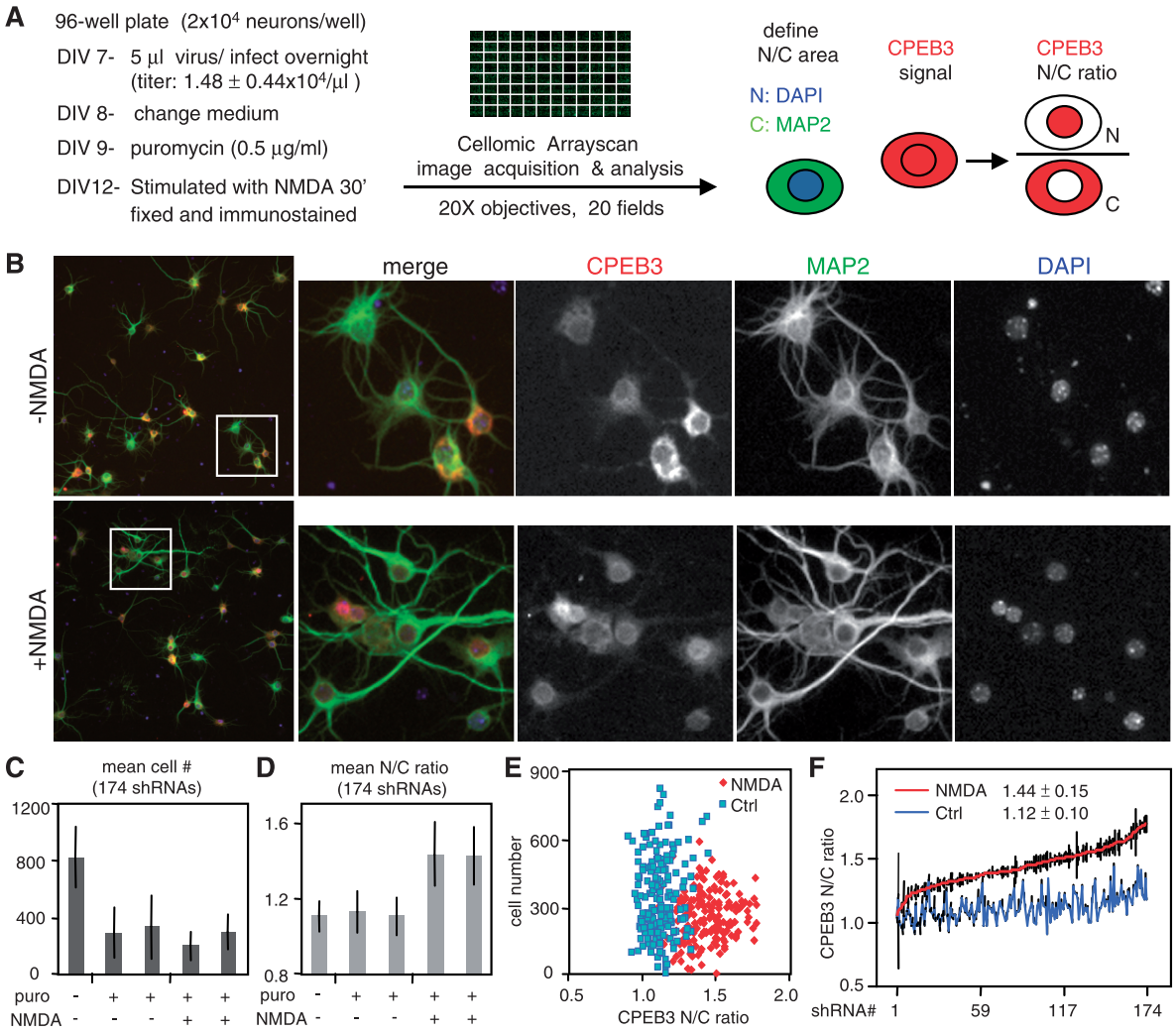


**G**

N/C ratio =<1.141 (1.44 - 1.96x0.15)

| Clone ID | Gene symbol | N/C ratio (mean± s.d.) | Analyzed cell # |
|---|---|---|---|
| TRCN0000070166 | Tnpo2 | 1.06 ±0.08 | 90/180 |
| TRCN0000079812 | Tnpo1 | 1.09 ± 0.64 | 39/357 |
| **TRCN0000101931** | **Ipo5** | **1.10±0.00** | **276/317** |
| TRCN0000101969 | Tnpo3 | 1.12±0.05 | 224/377 |
| **TRCN0000101932** | **Ipo5** | **1.14±0.01** | **310/467** |
| TRCN0000125910 | Phax | 1.14±0.25 | 1/269 |

N/C ratio >= 1.731 (1.44 + 1.96x0.15)

| Clone ID | Gene symbol | N/C ratio (mean± s.d.) | Analyzed cell # |
|---|---|---|---|
| TRCN0000093287 | Kpna6 | 1.75 ±0.08 | 134/271 |
| TRCN0000192647 | Ranbp3l | 1.75 ± 0.03 | 333/336 |
| TRCN0000093568 | Kpna3 | 1.76 ±0.04 | 109/195 |
| TRCN0000102843 | Ryr2 | 1.76 ±0.08 | 486/364 |
| TRCN0000174754 | Ranbp3 | 1.77 ±0.09 | 189/262 |
| TRCN0000102883 | Ryr3 | 1.77±0.09 | 279/328 |

**Figure 3.** Identification of the *trans*-acting molecules affecting nucleocytoplasmic distribution of CPEB3. (**A**) The scheme of virus-based shRNA knockdown screening to identify candidate karyopherins (see Supplementary Table S1 for all shRNA information). The neurons infected with lentiviruses expressing 174 shRNAs were stimulated with or without 20 µM NMDA and detected with MAP2 and CPEB3 antibodies and DAPI nuclear staining. N: nucleus; C: cytoplasm. Representative images from the screening are shown in (**B**). (**C**) The average cell number and (**D**) CPEB3 *N*/*C* ratio in each dataset (calculated from 174 shRNA's data) are displayed as bar graphs. (**E**) The cell numbers in each shRNA-infected well from duplicate datasets were averaged and plotted against the mean CPEB3 *N*/*C* ratio. (**F**) The mean CPEB3 *N*/*C* ratios obtained from 174 shRNA-targeted and NMDA-treated neurons are arranged in an increasing order (red line) and the ratios of their untreated counterparts are plotted in blue. The average CPEB3 *N*/*C* ratios from Ctrl- and NMDA-treated datasets are 1.12 ± 0.10 and 1.44 ± 0.15 (mean ± SD), respectively. (**G**) The shRNAs, which affect the CPEB3 *N*/*C* ratio beyond 95% confidence interval (mean ± 1.96 SD) in NMDA-stimulated neurons are listed. All error bars denote SD.

NMDA-increased nuclear CPEB3 signal is reduced greatly in neurons infected with two independent shRNAs designated against importin 5 (IPO5).

### Knockdown of IPO5 retards NMDA-induced nuclear accumulation of CPEB3

IPO5 belongs to the importin β superfamily of transport receptors (28). To evaluate whether IPO5 is indeed the transport receptor facilitating the nuclear import of CPEB3, we first examined the knockdown efficiency by western blotting using neurons infected with lentiviral particles expressing without (siCtrl) or with the two IPO5 shRNAs (siIPO5 #1 and #2, TRCN0000101932 and TRCN0000101931, respectively). The siCtrl (pLKO.1 vector) and siIPO5 lentiviral particles were prepared independently in the lab. Both shRNAs achieved ~50–60% knockdown efficiency (Figure 4A). The IPO5 shRNA #2 was then used in the following knockdown experiments. After puromycin selection to eliminate uninfected neurons, the siCtrl and siIPO5 neurons were treated with NMDA for the denoted time and then immunostained with CPEB3, IPO5, and MAP2 antibodies as well as DAPI. A line drawn across the cell body was analysed for CPEB3, IPO5, MAP2 and DAPI signals (Figure 4B). More sample images are shown in Supplementary Figure S2. The crossover point between DAPI (blue line) and MAP2 (yellow line) signals represents the nucleocytoplasmic border in each neuron (Figure 4B). The 7.2-μm-long fluorescent signal of CPEB3 on both sides (N: nucleus and C: cytoplasm) of the border in the siCtrl (red line) and siIPO5 (green line) neurons was measured and displayed as mean ± SEM (Figure 4C). The error bars for DAPI and MAP2 lines were omitted for simplification. Because the DAPI and MAP2 signals shown here represent averaged results, the crossover position is not exactly located at point 0. The sum of 7.2-μm-long nuclear versus cytoplasmic CPEB3 signal yields the $N/C$ ratio of each analysed neuron (Figure 4D). The average CPEB3 $N/C$ ratios in siCtrl and siIPO5 neurons stimulated without or with NMDA show that the NMDA-increased nuclear pool of CPEB3 is defective in siIPO5 neurons, except at the late time point (NMDA 45′, $P = 0.265$). It is likely that the remaining 40–50% of IPO5 proteins in siIPO5 neurons can facilitate CPEB3 import at a reduced rate. The IPO5 immunostained signal was also analysed. Interestingly, IPO5 is predominantly cytoplasmic unless treated with NMDA (Figure 4E and F). Using an alternative measurement, the results in this figure confirm that the knockdown of IPO5 decreases NMDA-induced nuclear distribution of CPEB3.

### IPO5 binds to RRM1 (NLS) of CPEB3 via its C-terminal cargo-binding domain

It is worth noting that long-term downregulation of karyopherins and transport regulatory proteins may have pleiotropic effects on neuronal physiology, e.g. impaired NMDA signaling, to affect nuclear import of CPEB3. In Figure 3G, Kpna6 and Kpna3 are also importins that facilitate nuclear localization of target proteins. Nonetheless, the nuclear CPEB3 signal was significantly elevated in these two shRNA knockdown neurons. That could be caused by secondary or RNAi off-target effects. Thus, if IPO5 is the *trans*-acting factor directly facilitating the nuclear translocation of CPEB3, it should bind to CPEB3 through the identified NLS in the RRM1 (Figure 2). To assess CPEB3–IPO5 interaction, HeLa cells expressing EGFP-IPO5 along with or without various myc-tagged CPEB3 mutants (Figure 5A) were either pulled down with GFP or myc antibody and immunodetected with GFP and myc antibodies. Co-IPs depict that IPO5 interacts with CPEB3 depending on RRM1, because wt, C and mut6, but not N and mut7, bind to IPO5 (Figure 5B). To map which region in IPO5 is essential for the association with CPEB3, HeLa cells expressing myc-CPEB3 and various EGFP-tagged truncated IPO5 mutants (Figure 5C) were precipitated with myc or GFP antibody and immunoblotted with GFP and myc antibodies. The cargo-binding domain (C1, a.a. 411–1115) of IPO5 is important for binding to CPEB3 (Figure 5D).

### NMDAR signaling facilitates nuclear import of CPEB3 by enhancing CPEB3–IPO5 interaction in a Ran-regulated manner

A significant decrease in the nuclear CPEB3 signal of NMDA-stimulated siIPO5 neurons (Figure 4D) suggests that NMDAR signaling likely accelerates nuclear translocation of CPEB3. To determine whether the increased nuclear signal is from trafficking of cytoplasmic or perhaps synaptic CPEB3, CPEB3 was fused with the photoconvertible fluorescent protein, Dendra2. Using Neuro-2a cells expressing Dendra2–CPEB3, it was possible to convert sufficient cytoplasmic Dendra2–CPEB3 and observe the nuclear accumulation of non-converted (green) and photoconverted (red) Dendra2–CPEB3 after LMB treatment (Supplementary Figure S3A). However, the expression level of Dendra2–CPEB3 in neurons was not high enough to detect converted fluorescent signal (Supplementary Figure S3B). Thus, we adopted an alternative approach to monitor the nuclearly accumulated signal of EGFP-CPEB3 in siCtrl or siIPO5 neurons stimulated with NMDA or LMB. We also traced the nuclear translocation of EGFP-IPO5, but no fluorescent signal in neurons or Neuro-2a cells expressing EGFP-IPO5 could be detected. This is likely because of the low expression level of EGFP-IPO5. In ~80% transfected Neuro-2a cells, the expression level of EGFP-IPO5 is lower than that of endogenous IPO5 and ectopically expressed EGFP-CPEB3 (Supplementary Figure S4). The experimental time frame is illustrated in Figure 6A. On DIV 14, the transfected neurons were recorded at 3 min interval for 30 min to acquire the baseline signal. After the addition of NMDA or LMB, the neurons were recorded for another 81–90 min. The sample images of EGFP-CPEB3 in NMDA-stimulated siCtrl and siIPO5 neurons are shown in Figure 6B. The time-lapse images from each recorded neuron with the designated nuclear region (circled in yellow, Figure 6B) were analysed. The nuclear EGFP-CPEB3 signal of each time frame averaged

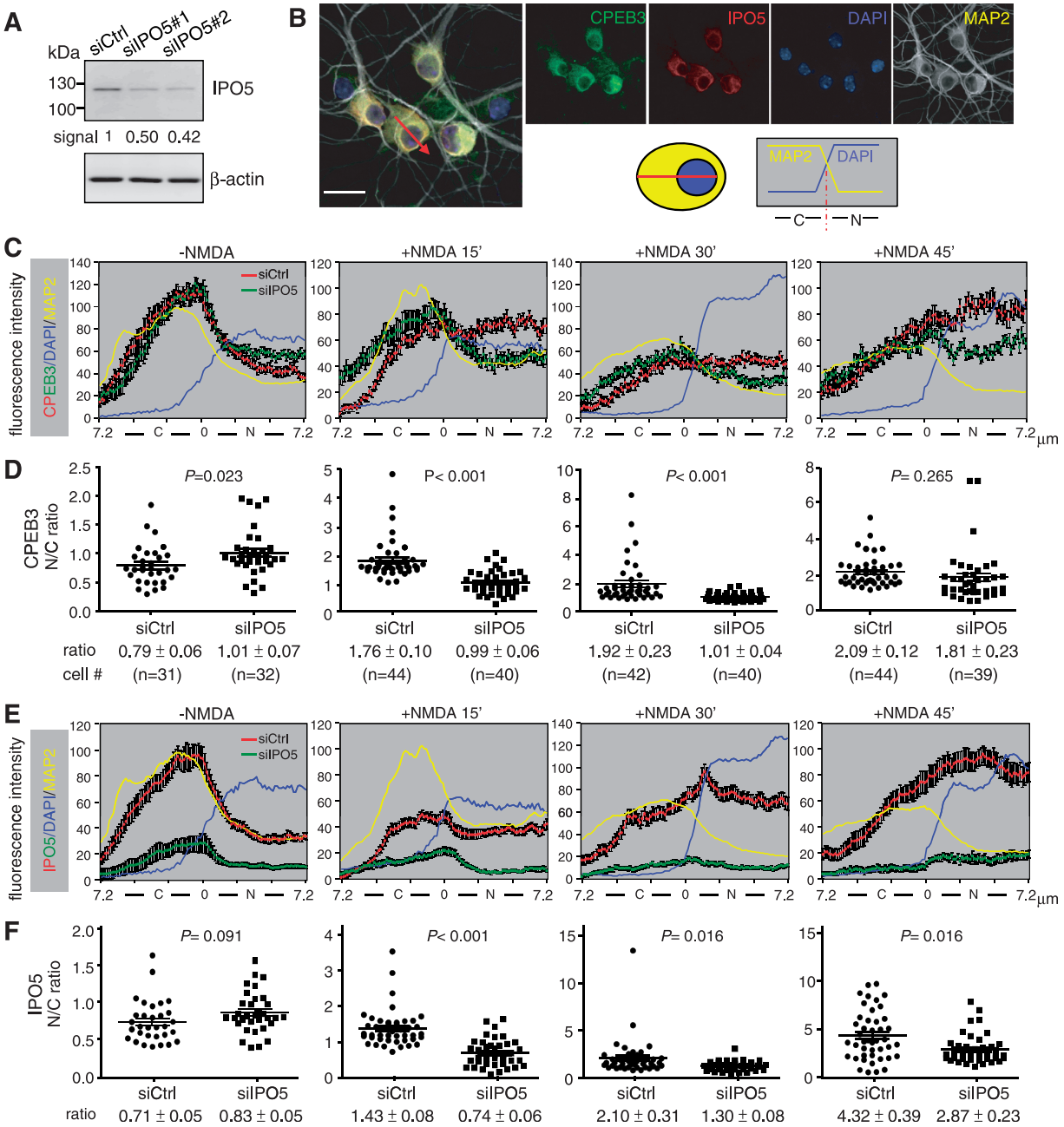


**Figure 4.** NMDA-induced nuclear accumulation of CPEB3 and IPO5 is impaired in IPO5 knockdown neurons. (**A**) Neurons infected with lentiviruses expressing without (siCtrl) or with IPO5 shRNAs, #1, TRCN00000101932 and #2, TRCN00000101931) were analysed by western blotting with IPO5 and actin antibodies. (**B**) The siCtrl and siIPO5 (#2 clone) neurons were treated with 20 µM NMDA for the indicated time courses and then immunostained with CPEB3, IPO5 and MAP2 antibodies and DAPI staining. The secondary antibodies used for CPEB3, IPO5 and MAP2 are conjugated with Alexa Fluor 546, Alexa Fluor 633 and FITC, respectively. The CPEB3 and IPO5 images are pseudo-coloured in green and red, respectively (see Supplementary Figure S2 for more images). A line drawn across the cell body was analysed for the fluorescence intensities of CPEB3, IPO5, MAP2 and DAPI. The nucleocytoplasmic border appears at the crossover point of MAP2 and DAPI signal lines. Scale: 20 µm (**C**) The 7.2 µm-long distance of cytoplasmic (C) and nuclear (N) CPEB3 signal in siCtrl (red line) and siIPO5 (green line) neurons treated with ± NMDA is plotted against distance. Error bars indicate SEM. The blue and yellow lines are the average DAPI (nucleus) and MAP2 (cytoplasm) signals. (**D**) For each neuron, the sum of 7.2 µm-long CPEB3 signal in the nucleus divided by that in the cytoplasm yields the *N*/*C* ratio in the dot plot. The quantified *N*/*C* ratio (mean ± SEM) and the number of analysed neurons are listed at the bottom. (**E** and **F**) The IPO5 signal was analysed in the same way.

from ~20 neurons under various experimental conditions is displayed as mean ± SEM. (Figure 6C). The increase of the nuclear EGFP-CPEB3 signal within 30 min after NMDA stimulation (red line) is reduced significantly in siIPO5 neurons (green line). Such a deficiency can be rescued with the expression of flag-tagged human IPO5 protein (yellow line). In contrast, blocking CRM1-dependent export with LMB also elevates nuclear

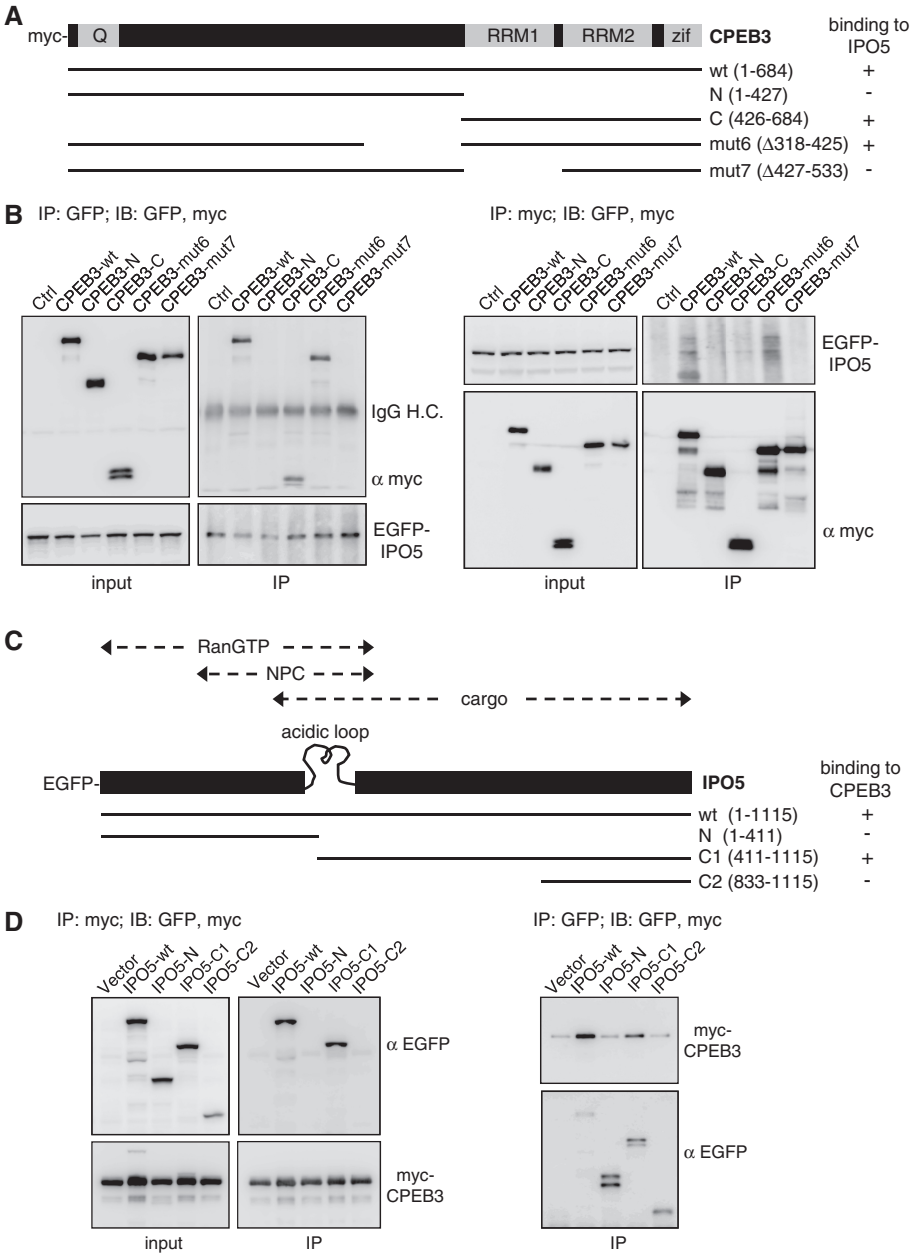


**Figure 5.** CPEB3 binds to the C-terminus of IPO5 through its RRM1. (**A**) The domain organization of CPEB3 and various truncated mutants. (**B**) Co-IP assay. HeLa cells were co-transfected with EGFP-IPO5 plasmid along with various myc-tagged CPEB3 constructs. The cell lysates were immunoprecipitated with GFP or myc antibody, and immunoblotted with myc and GFP antibodies. IP, immunoprecipitation; IB, immunoblotting. (**C**) The domain organization of IPO5 and various deleted mutants. NPC, nuclear pore complex. (**D**) HeLa cells expressing myc-CPEB3 along with various EGFP-tagged wt and mutant IPO5 proteins were pulled down by myc or GFP antibody. The precipitated substances were immunodetected with myc and GFP antibodies.

EGFP-CPEB3 level (i.e. dark blue line) with substantially less magnitude than NMDA stimulation (Figure 6C). This increase was slightly but significantly reduced within 20 min of LMB treatment in siIPO5 neurons (brown line), suggesting that IPO5 also facilitates the nuclear translocation of CPEB3 under unstimulated conditions (Figure 6C).

Live image analysis denotes that the NMDA-increased nuclear pool of CPEB3 is mostly contributed by IPO5-mediated import of CPEB3. Thus, we examined whether the association of CPEB3 and IPO5 increased in response to NMDA stimulation. Neurons with a 3 min pulse of NMDA were harvested at different time points for co-IP experiments. The neuronal lysates were divided and precipitated with CPEB3 and IPO5 IgGs, followed by immunoblotting with CPEB3, IPO5 and Ran antibodies. Using semi-quantitative measurements, both co-IPs show ~3–4-fold NMDA-enhanced binding of CPEB3 and IPO5 (Figure 7A). In contrast, the amount of Ran associated with IPO5 is not obviously

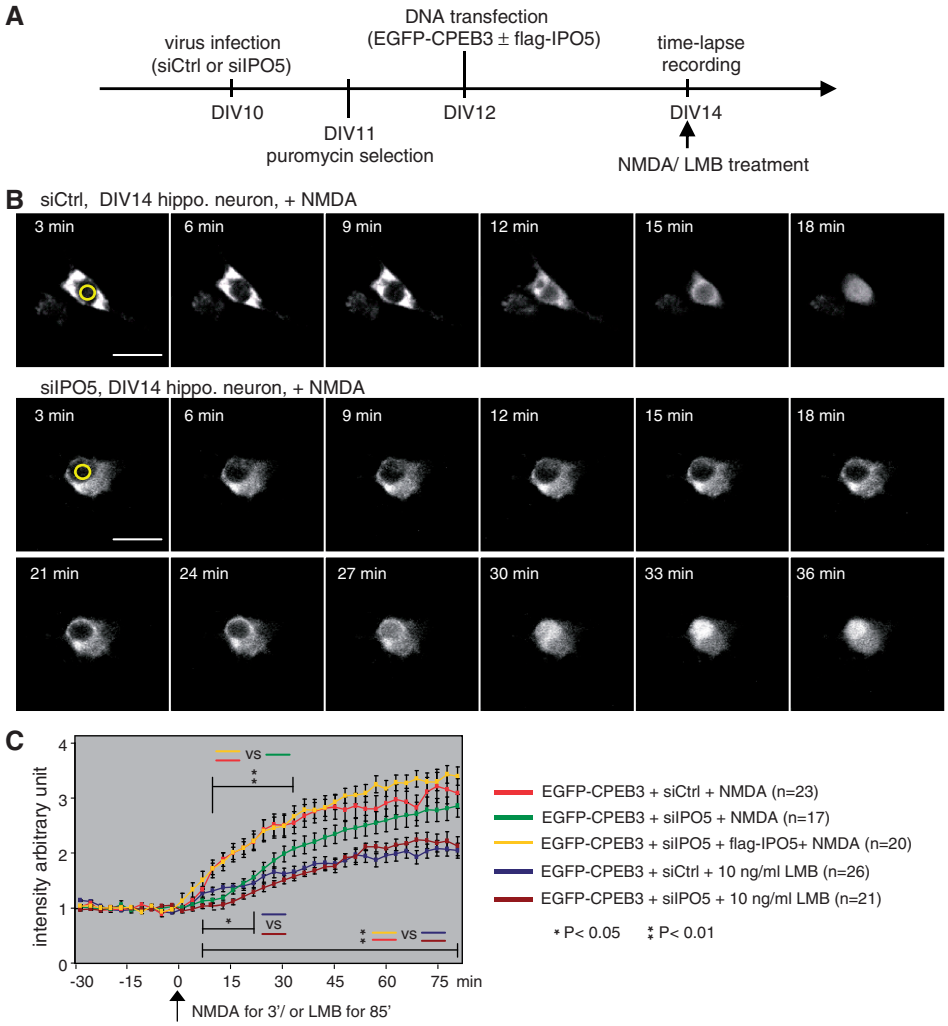


**Figure 6.** NMDAR signaling accelerates the nuclear import of CPEB3. (**A**) The scheme for live imaging of EGFP-CPEB3 import. (**B**) The siCtrl and siIPO5 neurons expressing EGFP-CPEB3 at DIV 14 were recorded for 30 min prior to stimulation with NMDA. Some time-lapse images are shown. Scale: 20 μm. The signal in the nuclear region circled in yellow was measured and (**C**) plotted against the time of recording with the fluorescence intensity at the middle of baseline (−15 min) arbitrarily set to one. The nuclear import dynamics of EGFP-CPEB3 under various conditions are shown in different colours. Error bars indicate SEM. The time windows showing statistical difference between groups are denoted (Student's *t*-test).

affected by NMDA (Figure 7A). This is also the case for CPEB3 and CRM1 interaction because the binding difference after NMDA stimulation is only ~10–30% (Supplementary Figure S5). IPO5 is a Ran-binding protein and its interaction with GTP- or GDP-bound Ran affects its cargo-binding and nuclear translocation activity (29,30). The co-precipitated Ran in the IPO5 pull-down (Figure 7A) is likely a mixture of RanGTP and RanGDP. Because NMDAR signaling also facilitates nuclear translocation of importins α1, α2 and β1 and their cargos, CREB2 and Jacob, we speculated whether a general mechanism, such as the GDP/GTP-binding ratio of Ran, may change in NMDA-treated neurons. The cytoplasmic extracts of neurons stimulated without or with NMDA were immunoprecipitated with an antibody recognizing RanGTP but not RanGDP. Although the total amount of Ran remains similar, the immunoprecipitated RanGTP level decreases slightly after NMDA activation (Figure 7B), implying that the RanGDP level is likely elevated. We then tested whether the Ran's nucleotide-bound state influenced the formation of the ternary complex of Ran, IPO5 and CPEB3. The exclusive GDP-binding (T24N) and GTPase-inactive (Q69L) Ran mutants, which are considered RanGDP and RanGTP locked forms of Ran, respectively (25), were used for co-IP experiments. The HeLa cells expressing myc-CPEB3, EGFP-IPO5 along with flag-tagged wt or mutant Ran were precipitated with flag (Figure 7C) or myc IgG (Figure 7D), followed by immunodetection with myc, GFP and flag antibodies. When equal amounts of wt and mutant Ran proteins were pulled down, ~2-fold more IPO5 was co-precipitated with RanGTP (Q69L) than RanGDP (T24N) (Figure 7C, IPO5/Ran). Of note, the amount of myc-CPEB3 in the RanGDP (T24N) complex with a reduced IPO5 level is similar to that in the RanGTP (Q69L) complex

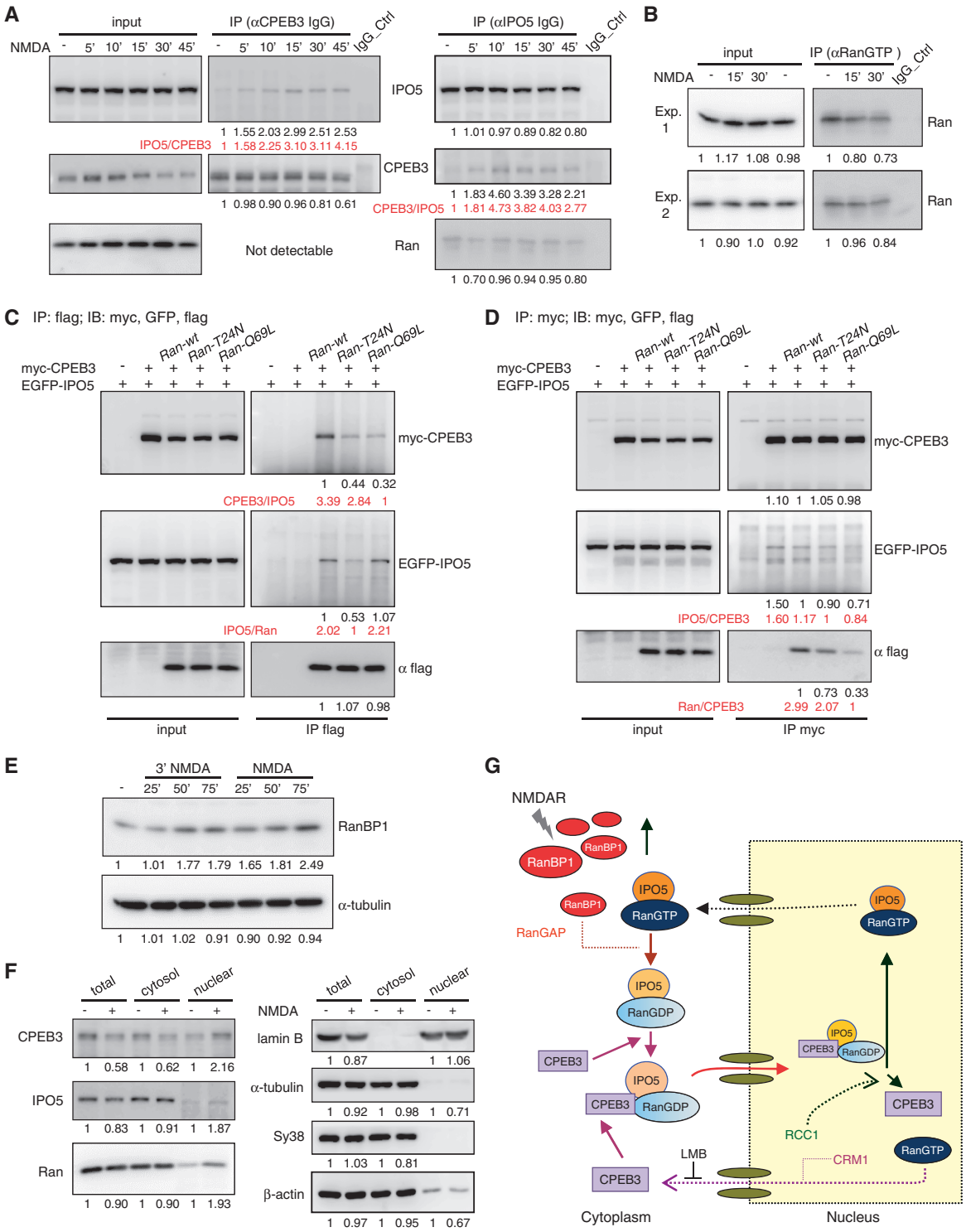


**Figure 7.** NMDAR signaling enhances CPEB3–IPO5 interaction through Ran-related changes. (**A**) Neurons stimulated with 3 min of NMDA and then incubated for the denoted time were used for IP with CPEB3 and IPO5 IgGs, followed by immunodetection with IPO5, CPEB3 and Ran antibodies. The intensities of immunodetected signals analysed by the ImageJ software are displayed as relative ratios at the bottoms of blots. The ratios of the co-precipitated target versus the immunoprecipitated protein (IPO5/CPEB3 or CPEB3/IPO5) are shown in red. (**B**) The cytoplasmic fraction isolated from neurons treated with ± NMDA was precipitated with the RanGTP antibody and immunoblotted with Ran antibody. (**C** and **D**) HeLa cells expressing myc-CPEB3, EGFP-IPO5 along with Ran-wt, T24N or Q69L mutant were pulled down with (**C**) flag or (**D**) myc antibodies. The precipitated substances were probed with GFP, myc and flag antibodies. (**E**) Neurons stimulated with a pulse of NMDA or NMDA for the indicated times were harvested for western blotting using RanBP1 and tubulin antibodies. (**F**) The nuclear and cytosol lysates fractionated from neurons treated with ± NMDA for 30 min were used for immunoblotting. (**G**) Schematic model of NMDA-induced nuclear import of CPEB3. NMDAR signaling increases RanBP1 expression, combined with RanGAP to stimulate Ran's GTPase activity. Consequently, the IPO5-RanGDP complex can bind to CPEB3 and deliver CPEB3 to the nucleus. After nuclear import, a high RanGTP concentration and RCC1 in the nucleus triggers the release of CPEB3 from the ternary complex because RanGTP impairs the interaction between IPO5 and CPEB3. The nuclear export of CPEB3 is mediated by CRM1.

(Figure 7C). After a semi-quantitative analysis, the ratio of CPEB3 versus IPO5 (CPEB3/IPO5) in the RanGDP (T24N) immunoprecipitated complex is near 3-fold higher than that in the RanGTP (Q69L) complex. Similarly, 2-fold more RanGDP (T24N) was indirectly co-precipitated with myc-CPEB3 (Figure 7D, Ran/CPEB3), suggesting that RanGDP-bound IPO5 has a higher affinity to CPEB3. The IP of wt Ran could pull down more myc-CPEB3 (Figure 7C) and vice versa (Figure 7D). Therefore, it is possible that the exchange of Ran in its GTP- or GDP-bound state could facilitate the ternary complex formation or not all mutant Ran proteins bind to guanine nucleotides, since Ran (T24N) mutant does not bind GTP and has a weak affinity for GDP (25). These results are in agreement with previous findings showing that IPO5 has higher affinity toward RanGTP, but binding of IPO5 to the cargo substrate requires the conversion of RanGTP to RanGDP (29,31,32). Similar to importin β, IPO5 preferentially binds RanGTP and stabilizes it against RanGAP1-induced GTP hydrolysis *in vitro*. The GAP resistance of the IPO5–RanGTP complex can be relieved by RanBP1 *in vitro* (29). To investigate whether RanBP1 expression is induced by NMDAR signaling, neurons treated with 3 min pulse of NMDA (a protocol to induce c-LTD) or continuously bathed in NMDA were harvested at the denoted time for western blotting. RanBP1 expression was elevated up to 2.5-fold in NMDA-stimulated neurons (Figure 7E), presumably leading to a reduction in the RanGTP level (Figure 7B). We also used the RanGTP antibody for immunostaining of neurons or Neuro-2a cells expressing wt, Q69L and T24N Ran proteins. However, this antibody produced no staining signal. Thus, we employed a different approach. The neurons treated with or without NMDA were fractioned for nuclear and cytosol lysates for western blotting (Figure 7F). Similar to CPEB3 and IPO5, there is concurrently increased nuclear Ran, implying that more Ran proteins are likely in the GDP-bound and import-proficient state. Together, the elevated expression of RanBP1 in NMDA-stimulated neurons increases the cytoplasmic RanGDP level. This in turn facilitates the formation of the CPEB3–IPO5–RanGDP ternary complex to accelerate the nuclear import of CPEB3 (Figure 7G).

## DISCUSSION

We have identified the molecular mechanism underlying the NMDA-induced nuclear import of CPEB3. IPO5, also known as RanBP5, importin β3 and karyopherin β3 (KPNB3), is the key *trans*-acting factor to facilitate the nuclear translocation of CPEB3 in NMDA-treated neurons. Because CPEB3 plays a cytoplasmic role in translation and a nuclear role in transcription, the activity-induced change in CPEB3 localization may partition CPEB3's function in translation and transcription. Because CPEB3 is localized in the synaptodendritic region (17), CPEB3 may also be transported from NMDAR-activated synapses into the nucleus to engage and facilitate the dendritic transport of its target RNAs. Whether CPEB3 plays a role in dendritic RNA transport similar to CPEB1 (33) and the physiological significance of NMDA-induced nuclear import of CPEB3 both require further investigation.

Unlike classical importins α1, α2 and β1, IPO5 is predominantly localized in the cytoplasm, and NMDA stimulation induces its nuclear translocation. Previous research has shown that the subcellular distribution of IPO5 can shift between the nucleus and the cytoplasm in fetal germ cells in an age- and sex-specific manner (34). Thus, the cargo-transporting activity of IPO5 to the nucleus can be regulated by different developmental cues and neuronal signaling. IPO5 is also essential for the life cycle of influenza A virus and human papillomavirus-16 because it shuttles specific viral proteins into the nucleus (35,36). In addition, the nuclear import of several ribosomal subunits, L7, L5, L23a and S7, is partially mediated by IPO5 (30,31). IPO5 binds to substrates with high affinity when in complex with RanGDP but not RanGTP (29,31). Here, we find NMDAR signaling increases the expression of RanBP1, which presumably enhances the nuclear translocation and cargo-binding activity of IPO5 to facilitate CPEB3 import. This is because the binding of RanBP1 to the IPO5-RanGTP complex allows efficient stimulation of hydrolysis of Ran-bound GTP by RanGAP1 (29). Although several studies indicate that KPNB3 locus (i.e. IPO5) is associated with schizophrenia (37–40), IPO5 has not been studied in neurons to assess its potential involvement in this disease. It will be of interest to understand the role of IPO5 in activity-dependent nuclear import in neurons, including identification of the additional cargos other than CPEB3 carried by IPO5.

After prolonged activation of NMDA receptors, which eventually leads to excitotoxicity-induced neuronal death, or when using a protocol that evokes chemical LTD (c-LTD), CPEB3 accumulates in the nucleus by enhancing IPO5-mediated import of CPEB3. The association of importins with GDP-bound or GTP-bound Ran affects their affinity to cargo proteins and the efficiency of nuclear translocation. These functions are controlled by a gradient of RanGTP to RanGDP, established by the spatial separation of a RanGAP (i.e. RanGAP1) in the cytoplasm and a RanGEF (i.e. RCC1) in the nucleus (26,41,42). Interestingly, recent findings suggest that the RanGTP/RanGDP ratio can be regulated by local synthesis of RanBP1 in injured axons (13). An additional Ran-binding protein, RanBP10, acting as a cytoplasmic RanGEF in megakaryocytes has been reported (43). Thus, the guanine nucleotide-binding state of Ran can be regulated spatially in the cytoplasm. Such a change may also underlie the increased nuclear shuttling of CREB2 and Jacob mediated by the classical importin pathway in NMDA-activated neurons (8,44). Although the nuclear translocation of Jacob can be induced in the prolonged NMDA-treated neurons, only chemical long-term potentiation (c-LTP) but not c-LTD can drive nuclear translocation of Jacob (7,44). In contrast, we also observed that CPEB3, similar to CREB2, was nuclearly accumulated under c-LTD but not c-LTP. If the activation of NMDA receptors increases RanBP1 expression

that can shift Ran's nucleotide-bound state to RanGDP, are all importin-mediated pathways simultaneously activated to direct a huge influx of diverse cargos to the nucleus? This scenario may exist under pathological conditions in which synaptic and extra-synaptic NMDARs are activated extensively. However, under physiological conditions (i.e. synaptic transmission), the spatial restriction and temporal stimulation of NMDA receptors limits the change of Ran's GDP/GTP-bound state only in the activated synaptic areas to an extent that may influence some importins but not others. For example, RanBP1 can stimulate hydrolysis of Ran-bound GTP in the IPO5–RanGTP–RanGAP1 complex 50-fold more than that in the importin β–RanGTP–RanGAP1 complex *in vitro* (29). A slight change in the RanBP1 level should affect the dynamics of IPO5 more than importin β *in vivo*. Moreover, the binding affinity of individual importin for RanGTP and RanGDP varies, such as the affinity of RanBP7 to RanGTP is ~30-fold lower than that of importin β (30). Other than the differences in importins, some cargos may use additional regulations to control retrograde translocation. For example, the cleavage of myristoylated N-terminus of Jacob is required to relieve its membrane anchorage prior to nuclear translocation (7). The $Ca^{2+}$-binding protein caldendrin can compete with importin α for binding to the NLS of Jacob to control the extra-nuclear localization of Jacob (15). Thus, depending on the specific signal initiators, nuclear translocators, Ran modulators, and cargos, the nucleus can receive the diverse synaptic information through specifically imported cytoplasmic cargos. The balance between the nuclear and cytoplasmic pool of CPEB3 likely dictates CPEB3's function in the two compartments to control gene expression.

## SUPPLEMENTARY DATA

Supplementary Data are available at NAR Online: Supplementary Table 1, Supplementary Figures 1–5 and Supplementary Data.

## ACKNOWLEDGEMENTS

The authors thank Joel Richter for polyclonal CPEB3 antibody, Yi-Ping Hsueh for lamin B antibody, Chiaho Shih for CRM1 antibody, Dirk Gorlich for the pQE30-IPO5 plasmid and Mien-Chie Hung for pcDNA3.1-flag-Ran and pcDNA3.1-flag-RanQ69L plasmids. They appreciate Thomas Nieland and David Root for helping to establish the shRNA screening protocol and Sue-Ping Lee's assistance with the confocal image analysis. They thank the National RNAi Core Facility in Academia Sinica for the shRNA viruses and clones.

## FUNDING

National Science Council [NSC 99-2311-B-001-020-MY3]; National Health Research Institute [NHRI-EX101-9814NI]; Academia Sinica [AS-100-TP-B09] in Taiwan. The RNAi Core supported by the National Research Program for Genomic Medicine Grants is also gratefully acknowledged. Funding for open access charge: National Science Council, Taiwan.

*Conflict of interest statement*. None declared.

## REFERENCES

1. Gkogkas,C., Sonenberg,N. and Costa-Mattioli,M. (2010) Translational control mechanisms in long-lasting synaptic plasticity and memory. *J. Biol. Chem.*, **285**, 31913–31917.
2. Loebrich,S. and Nedivi,E. (2009) The function of activity-regulated genes in the nervous system. *Physiol. Rev.*, **89**, 1079–1103.
3. Richter,J.D. and Klann,E. (2009) Making synaptic plasticity and memory last: mechanisms of translational regulation. *Genes Dev.*, **23**, 1–11.
4. Jordan,B.A. and Kreutz,M.R. (2009) Nucleocytoplasmic protein shuttling: the direct route in synapse-to-nucleus signaling. *Trends Neurosci.*, **32**, 392–401.
5. Otis,K.O., Thompson,K.R. and Martin,K.C. (2006) Importin-mediated nuclear transport in neurons. *Curr. Opin. Neurobiol.*, **16**, 329–335.
6. Kan,M.C., Oruganty-Das,A., Cooper-Morgan,A., Jin,G., Swanger,S.A., Bassell,G.J., Florman,H., van Leyen,K. and Richter,J.D. (2010) CPEB4 is a cell survival protein retained in the nucleus upon ischemia or endoplasmic reticulum calcium depletion. *Mol. Cell Biol.*, **30**, 5658–5671.
7. Kindler,S., Dieterich,D.C., Schutt,J., Sahin,J., Karpova,A., Mikhaylova,M., Schob,C., Gundelfinger,E.D., Kreienkamp,H.J. and Kreutz,M.R. (2009) Dendritic mRNA targeting of Jacob and *N*-methyl-*d*-aspartate-induced nuclear translocation after calpain-mediated proteolysis. *J. Biol. Chem.*, **284**, 25431–25440.
8. Lai,K.O., Zhao,Y., Ch'ng,T.H. and Martin,K.C. (2008) Importin-mediated retrograde transport of CREB2 from distal processes to the nucleus in neurons. *Proc. Natl Acad. Sci. USA*, **105**, 17175–17180.
9. Peng,S.C., Lai,Y.T., Huang,H.Y., Huang,H.D. and Huang,Y.S. (2010) A novel role of CPEB3 in regulating EGFR gene transcription via association with Stat5b in neurons. *Nucleic Acids Res.*, **38**, 7446–7457.
10. Flavell,S.W. and Greenberg,M.E. (2008) Signaling mechanisms linking neuronal activity to gene expression and plasticity of the nervous system. *Annu. Rev. Neurosci.*, **31**, 563–590.
11. Bilokapic,S. and Schwartz,T.U. (2012) 3D ultrastructure of the nuclear pore complex. *Curr. Opin. Cell. Biol.*, **24**, 86–91.
12. Thompson,K.R., Otis,K.O., Chen,D.Y., Zhao,Y., O'Dell,T.J. and Martin,K.C. (2004) Synapse to nucleus signaling during long-term synaptic plasticity; a role for the classical active nuclear import pathway. *Neuron*, **44**, 997–1009.
13. Yudin,D., Hanz,S., Yoo,S., Iavnilovitch,E., Willis,D., Gradus,T., Vuppalanchi,D., Segal-Ruder,Y., Ben-Yaakov,K., Hieda,M. *et al.* (2008) Localized regulation of axonal RanGTPase controls retrograde injury signaling in peripheral nerve. *Neuron*, **59**, 241–252.
14. Ben-Yaakov,K., Dagan,S.Y., Segal-Ruder,Y., Shalem,O., Vuppalanchi,D., Willis,D.E., Yudin,D., Rishal,I., Rother,F., Bader,M. *et al.* (2012) Axonal transcription factors signal retrogradely in lesioned peripheral nerve. *EMBO J.*, **31**, 1350–1363.
15. Dieterich,D.C., Karpova,A., Mikhaylova,M., Zdobnova,I., Konig,I., Landwehr,M., Kreutz,M., Smalla,K.H., Richter,K., Landgraf,P. *et al.* (2008) Caldendrin-Jacob: a protein liaison that couples NMDA receptor signalling to the nucleus. *PLoS Biol.*, **6**, e34.
16. Chen,P.J. and Huang,Y.S. (2012) CPEB2-eEF2 interaction impedes HIF-1alpha RNA translation. *EMBO J.*, **31**, 959–971.
17. Huang,Y.S., Kan,M.C., Lin,C.L. and Richter,J.D. (2006) CPEB3 and CPEB4 in neurons: analysis of RNA-binding specificity and translational control of AMPA receptor GluR2 mRNA. *EMBO J.*, **25**, 4865–4876.

18. Lin,C.L., Evans,V., Shen,S., Xing,Y. and Richter,J.D. (2010) The nuclear experience of CPEB: implications for RNA processing and translational control. *RNA*, **16**, 338–348.
19. Goldberg,W.J., Kadingo,R.M. and Barrett,J.N. (1986) Effects of ischemia-like conditions on cultured neurons: protection by low $Na^+$, low $Ca2^+$ solutions. *J. Neurosci.*, **6**, 3144–3151.
20. Monyer,H., Giffard,R.G., Hartley,D.M., Dugan,L.L., Goldberg,M.P. and Choi,D.W. (1992) Oxygen or glucose deprivation-induced neuronal injury in cortical cell cultures is reduced by tetanus toxin. *Neuron*, **8**, 967–973.
21. Huang,Y.S. and Richter,J.D. (2007) Analysis of mRNA translation in cultured hippocampal neurons. *Methods Enzymol.*, **431**, 143–162.
22. Banker,G. and Goslin,K. (1988) Developments in neuronal cell culture. *Nature*, **336**, 185–186.
23. Jiang,M. and Chen,G. (2006) High Ca2+-phosphate transfection efficiency in low-density neuronal cultures. *Nat. Protoc.*, **1**, 695–700.
24. Root,D.E., Hacohen,N., Hahn,W.C., Lander,E.S. and Sabatini,D.M. (2006) Genome-scale loss-of-function screening with a lentiviral RNAi library. *Nat. Methods*, **3**, 715–719.
25. Clarke,P.R. and Zhang,C. (2001) Ran GTPase: a master regulator of nuclear structure and function during the eukaryotic cell division cycle? *Trends Cell Biol.*, **11**, 366–371.
26. Bischoff,F.R., Klebe,C., Kretschmer,J., Wittinghofer,A. and Ponstingl,H. (1994) RanGAP1 induces GTPase activity of nuclear Ras-related Ran. *Proc. Natl Acad. Sci. USA*, **91**, 2587–2591.
27. Bischoff,F.R. and Ponstingl,H. (1991) Catalysis of guanine nucleotide exchange on Ran by the mitotic regulator RCC1. *Nature*, **354**, 80–82.
28. Strom,A.C. and Weis,K. (2001) Importin-beta-like nuclear transport receptors. *Genome Biol.*, **2**, REVIEWS3008.
29. Deane,R., Schafer,W., Zimmermann,H.P., Mueller,L., Gorlich,D., Prehn,S., Ponstingl,H. and Bischoff,F.R. (1997) Ran-binding protein 5 (RanBP5) is related to the nuclear transport factor importin-beta but interacts differently with RanBP1. *Mol. Cell Biol.*, **17**, 5087–5096.
30. Jakel,S. and Gorlich,D. (1998) Importin beta, transportin, RanBP5 and RanBP7 mediate nuclear import of ribosomal proteins in mammalian cells. *EMBO J.*, **17**, 4491–4502.
31. Chou,C.W., Tai,L.R., Kirby,R., Lee,I.F. and Lin,A. (2010) Importin beta3 mediates the nuclear import of human ribosomal protein L7 through its interaction with the multifaceted basic clusters of L7. *FEBS Lett.*, **584**, 4151–4156.
32. Deng,T., Engelhardt,O.G., Thomas,B., Akoulitchev,A.V., Brownlee,G.G. and Fodor,E. (2006) Role of ran binding protein 5 in nuclear import and assembly of the influenza virus RNA polymerase complex. *J. Virol.*, **80**, 11911–11919.
33. Huang,Y.S., Carson,J.H., Barbarese,E. and Richter,J.D. (2003) Facilitation of dendritic mRNA transport by CPEB. *Genes Dev.*, **17**, 638–653.
34. Hogarth,C.A., Jans,D.A. and Loveland,K.L. (2007) Subcellular distribution of importins correlates with germ cell maturation. *Dev. Dyn.*, **236**, 2311–2320.
35. Hutchinson,E.C., Orr,O.E., Man Liu,S., Engelhardt,O.G. and Fodor,E. (2011) Characterization of the interaction between the influenza A virus polymerase subunit PB1 and the host nuclear import factor Ran-binding protein 5. *J. Gen. Virol.*, **92**, 1859–1869.
36. Nelson,L.M., Rose,R.C. and Moroianu,J. (2003) The L1 major capsid protein of human papillomavirus type 11 interacts with Kap beta2 and Kap beta3 nuclear import receptors. *Virology*, **306**, 162–169.
37. Hu,Y., Liu,L., Ju,G., Zhang,X., Xie,L., Liu,S., Shi,J., Yu,Y., Sun,Z., Guo,Y. *et al.* (2005) An association study of the KPNB3 locus with schizophrenia in a Chinese population. *Schizophr. Res.*, **76**, 363–365.
38. Liu,L.B., Hu,Y., Ju,G.Z., Zhang,X., Xie,L., Liu,S.Z., Shi,J.P., Yu,Y.Q., Xu,Q., Fan,Y. *et al.* (2007) Is KPNB3 locus associated with schizophrenia? *Biomed. Environ. Sci.*, **20**, 52–55.
39. Wei,J. and Hemmings,G.P. (2004) The KPNB3 locus is associated with schizophrenia. *Neurosci. Lett.*, **368**, 323–326.
40. Zhang,H., Ju,G., Wei,J., Hu,Y., Liu,L., Xu,Q., Chen,Y., Sun,Z., Liu,S., Yu,Y. *et al.* (2006) A combined effect of the KPNA3 and KPNB3 genes on susceptibility to schizophrenia. *Neurosci. Lett.*, **402**, 173–175.
41. Gorlich,D., Pante,N., Kutay,U., Aebi,U. and Bischoff,F.R. (1996) Identification of different roles for RanGDP and RanGTP in nuclear protein import. *EMBO J.*, **15**, 5584–5594.
42. Klebe,C., Bischoff,F.R., Ponstingl,H. and Wittinghofer,A. (1995) Interaction of the nuclear GTP-binding protein Ran with its regulatory proteins RCC1 and RanGAP1. *Biochemistry*, **34**, 639–647.
43. Schulze,H., Dose,M., Korpal,M., Meyer,I., Italiano,J.E. Jr and Shivdasani,R.A. (2008) RanBP10 is a cytoplasmic guanine nucleotide exchange factor that modulates noncentrosomal microtubules. *J. Biol. Chem.*, **283**, 14109–14119.
44. Behnisch,T., Yuanxiang,P., Bethge,P., Parvez,S., Chen,Y., Yu,J., Karpova,A., Frey,J.U., Mikhaylova,M. and Kreutz,M.R. (2011) Nuclear translocation of jacob in hippocampal neurons after stimuli inducing long-term potentiation but not long-term depression. *PLoS One*, **6**, e17276.